Available online at www.sciencedirect.com

ScienceDirect

Journal of Bionic Engineering 9 (2012) 211–223

Can Quick Release Experiments Reveal the Muscle Structure? A Bionic Approach

D. F. B. Haeufle[1,2], M. Günther[1,2], R. Blickhan[3], S. Schmitt[1,2]

1. *Institute of Sports and Exercise-Science*, *University of Stuttgart*, *Allmandring* 28, D-70569 *Stuttgart*, *Germany*
2. *Stuttgart Research Centre for Simulation Technology* (*SRC SimTech*), *University of Stuttgart*, *Pfaffenwaldring* 7a, D-70569 *Stuttgart*, *Germany*
3. *Institute of Motion Science*, *Friedrich-Schiller-University*, *Seidelstraße* 20, D-07749 *Jena*, *Germany*

Abstract

The goal of this study was to understand the macroscopic mechanical structure and function of biological muscle with respect to its dynamic role in the contraction. A recently published muscle model, deriving the hyperbolic force-velocity relation from first-order mechanical principles, predicts different force-velocity operating points for different load situations. With a new approach, this model could be simplified and thus, transferred into a numerical simulation and a hardware experiment. Two types of quick release experiments were performed in simulation and with the hardware setup, which represent two extreme cases of the contraction dynamics: against a constant force (isotonic) and against an inertial mass. Both experiments revealed hyperbolic or hyperbolic-like force-velocity relations. Interestingly, the analytical model not only predicts these extreme cases, but also additionally all contraction states in between. It was possible to validate these predictions with the numerical model and the hardware experiment. These results prove that the origin of the hyperbolic force-velocity relation can be mechanically explained on a macroscopic level by the dynamical interaction of three mechanical elements. The implications for the interpretation of biological muscle experiments and the realization of muscle-like bionic actuators are discussed.

Keywords: force-velocity relation, isotonic, quick release, proof of concept, artificial muscle

doi: 10.1016/S1672-6529(11)60115-7

1 Introduction

Work has been ongoing for decades to reveal the functional principles of biological muscles. The basis of this work is the knowledge from a variety of well defined muscle experiments performed with isolated muscles[1,2] or muscle fibers[3]. Typical muscle experiments are isometric, isokinetic, and quick release experiments. Isometric contractions are used to reveal the force-length dependency in muscle contraction[4,5]. Isokinetic contractions[2,6–9], isotonic quick release experiments[2,10–12] and quick release contractions against an inertial mass[13,14] are used to determine the dynamic properties of muscles, namely, the force-velocity dependency. Each of these experiments is repeated several times, the isotonic experiments at several lengths, and the dynamic contractions for varying external loads and/or velocities. The force-length and force-velocity relations can only be determined from such a set of experiments, as each experimental condition retrieves one operating point of the muscle.

To interpret the experimental results quantitatively and find the underlying mechanisms, many muscle models were introduced. Microscopic Huxley-type muscle models allow to account for the sub-cellular and molecular origin of global muscle contraction dynamics[15–23]. With at least 30 parameters in the more recent approaches and several coupled differential and rate equations, such models can predict the force-velocity characteristics of a half sarcomere (smallest structural unit in the muscle). Macroscopic Hill-type muscle models on the other hand can predict the overall force production of a muscle or a muscle tendon complex[1,8,14,24–26]. Here, the force-length and force-velocity characteristics as known from the experiments are implemented as phenomenological relations in a so-called

Corresponding author: D. F. B. Haeufle
E-mail: daniel.haeufle@inspo.uni-stuttgart.de

Contractile Element (CE). By integrating such muscle models in musculo-skeletal models it is possible to investigate biological movement generation in forward dynamics simulations[26–31] and estimate internal forces in inverse dynamics simulations[32,33].

Muscle models, defining the non-linear dynamic characteristics of biological muscle, enable to ask for the functional role that specific muscle characteristics play in the context of movement generation and control. At least three important features are well reported in literature: several studies emphasize the importance of the force-velocity relation for the stabilization of movements[26,34–37], the elastic properties of muscles are relevant for energy efficient locomotion[38,39] and shock protection[40–42].

In extension to numerical simulations, robots are used to study human and animal movement[43–48]. If the intrinsic muscle properties play a crucial role, such robots need bionic actuators with muscle-like contraction dynamics in order to correctly represent the crucial mechanisms for the evaluation of bio-inspired control approaches. Elasticity can be introduced by mechanical elements[49–52], but the phenomenological force-velocity characteristics could so far not be reproduced accurately as an intrinsic actuator property. A basis for adequate actuators could be a new design concept published recently[53]. This design concept proposed three simple mechanical elements, an active element as energy source, a parallel damper and a serial element. In contrast to the previous phenomenological models, this approach allowed for an analytical deduction of the hyperbolic force-velocity relation from the physical properties of the elements. With a first hardware implementation of the concept a set of quick release experiments against an inertial mass was performed[54]. There, it was only possible to qualitatively reproduce a hyperbolic force-velocity relation, which quantitatively deviated from the theory.

Here, we present a modification to the theory of Ref. [53], which, in fact, is a simplification enabling a fully consistent comparison of quick-release experiments in a bionic approach. The theory analytically predicts hyperbolic force-velocity relations for different contraction modes. The goal of this study was to verify the analytical predictions in a numerical model and a hardware implementation and understand the relationship between the macroscopic model structure and its dynamic role in the contraction. Therefore, two types of quick release experiments were performed in simulation and hardware, which represent two extreme cases of the contraction dynamics: against a constant force (isotonic) and against an inertial mass. Interestingly, the new theory predicts all states in between these extreme cases and it was possible to validate these predictions with the numerical model and the hardware experiment. The implications for the simulation of dynamic musculo-skeletal movements, for biological muscle experiments, and for the realization of muscle-like bionic actuators are discussed.

2 Methods

2.1 New formulation of the theory

In a recent paper[53] it was demonstrated that the phenomenologically found[1] hyperbolic force-velocity relation of a concentrically contracting assembly of activated muscle fibers, Contractile Element (CE), can be derived from the combination of three simple mechanical elements: an arbitrary force generating Active Element (AE) to which a damper (PDE) is connected in parallel and, in series to both, a Serial Element (SE) (Fig. 1). The three elements fulfill the force equilibrium

$$F_{\mathrm{CE}} = F_{\mathrm{SE}} = F_{\mathrm{AE}} + F_{\mathrm{PDE}}, \tag{1}$$

where the symbol F denotes the force produced by each element as referred to by a corresponding index. The kinematic relation for the lengths l of the elements is

$$l_{\mathrm{AE}} = l_{\mathrm{PDE}} = l_{\mathrm{CE}} - l_{\mathrm{SE}}. \tag{2}$$

Note that a dot symbol $\dot{l}$ denotes the first time derivative of a length l, i.e. an element's contraction velocity. The kinematic gearing ratio between internal (SE) and external (CE) contraction velocities can be represented by an arbitrary parameter

$$\kappa_v = \frac{\dot{l}_{\mathrm{SE}}}{\dot{l}_{\mathrm{CE}}}. \tag{3}$$

The only element that is explicitly specified is the PDE. The force of the PDE is assumed to be

$$F_{\mathrm{PDE}} = d_{\mathrm{PDE}} \cdot \dot{l}_{\mathrm{PDE}}, \tag{4}$$

where the damping coefficient d_{PDE} of the PDE depends linearly on the current CE force F_{CE}:

$$d_{\mathrm{PDE}}(F_{\mathrm{CE}}) = D_{\mathrm{PDE,max}} \cdot ((1 - R_{\mathrm{PDE}}) \cdot \frac{F_{\mathrm{CE}}}{F_{\mathrm{AE,max}}} + R_{\mathrm{PDE}}), \tag{5}$$

where $D_{\mathrm{PDE,max}}$ is the maximum damping coefficient (at $F_{\mathrm{CE}} = F_{\mathrm{AE,max}}$) and R_{PDE} the normalized (to $D_{\mathrm{PDE,max}}$) minimum (force independent) value of $d_{\mathrm{PDE}}(F_{\mathrm{CE}})$. The characteristics of the SE do not have to be specified.

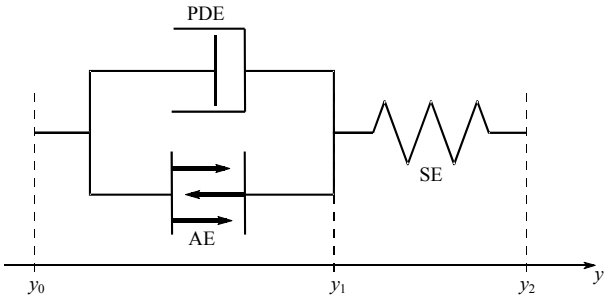

Fig. 1 Theoretical construct of the CE[53]. The CE consists of three elements: active element AE, parallel damping element PDE, and serial element SE. $y_0 = 0$ is the origin of the CE, y_1 represents the length of the AE/PDE and y_2 the length of the whole CE.

The AE is the source of mechanical energy. For this element, we simplify the approach of Ref. [53]: we now assume the straight forward identity

$$F_{\mathrm{AE}} = q_{\mathrm{AE}} \cdot F_{\mathrm{AE,max}} = F_{\mathrm{CE},0}, \tag{6}$$

with $F_{\mathrm{AE,max}}$ being the maximum AE force, $0 \le q_{\mathrm{AE}} \le 1$ representing the activity of the muscle[24], and $F_{\mathrm{CE},0}$ denoting the isometric CE force. This is in contrast to Eq. (6) in Ref. [53], where the AE force depended on SE length and the damping coefficient: $F_{\mathrm{AE}} = F_{\mathrm{CE},0} + d_{\mathrm{PDE}}(F_{\mathrm{CE},0}) \cdot \dot{l}_{\mathrm{SE}}$. Here, the force of the AE and the isometric force of the CE ($F_{\mathrm{CE},0} = F_{\mathrm{CE}}(\dot{l}_{\mathrm{CE}} = 0)$) are simply assumed to be the same input parameter with no dependencies: $F_{\mathrm{AE}} = F_{\mathrm{CE},0}$.

All simulations and experiments were performed with full activity $q_{\mathrm{AE}} = 1$. This is equal to the assumption that the muscle fibers are maximally activated and operate at optimal length throughout the experiments, as usually assumed for quick release experiments.

This simplification allows a straight forward numerical and hardware implementation, but also changes the derivation of the hyperbolic force-velocity relation: Substituting Eq. (4), the explicit dependency of $d_{\mathrm{PDE}}(F_{\mathrm{AE}})$ on force F_{AE} and model parameters (Eq. (5)), and Eq. (3) into Eq. (1), thereby considering the time derivative of Eq. (2), makes the force equilibrium Eq. (1) to constitute a hyperbola

$$\begin{aligned}(F_{\mathrm{CE}} + \frac{R_{\mathrm{PDE}}}{1-R_{\mathrm{PDE}}} \cdot F_{\mathrm{AE,max}}) \cdot \dot{l}_{\mathrm{CE}} = \\ -\frac{1}{1-R_{\mathrm{PDE}}} \cdot \frac{1}{1-\kappa_v} \cdot \frac{F_{\mathrm{AE,max}}}{D_{\mathrm{PDE,max}}} \cdot (F_{\mathrm{AE,max}} - F_{\mathrm{CE}}).\end{aligned} \tag{7}$$

Comparing this hyperbola to the original formulation of Hill[1]

$$(F_{\mathrm{CE}} + A) \cdot \dot{l}_{\mathrm{CE}} = -B \cdot (F_{\mathrm{CE},0} - F_{\mathrm{CE}}), \tag{8}$$

with the Hill parameters A, B and the isometric force $F_{\mathrm{CE},0}$ being positive and $\dot{l}_{\mathrm{CE}}$ consistently being negative in the shortening (concentric) case, the Hill parameters can be expressed in terms of the new mechanical parameters

$$A = \frac{R_{\mathrm{PDE}}}{1-R_{\mathrm{PDE}}} \cdot F_{\mathrm{AE,max}}, \tag{9}$$

$$B = \frac{1}{1-R_{\mathrm{PDE}}} \cdot \frac{1}{1-\kappa_v} \cdot \frac{F_{\mathrm{AE,max}}}{D_{\mathrm{PDE,max}}}. \tag{10}$$

2.2 Deriving the mechanical parameters

Through Eqs. (9) and (10) the Hill parameters A and B are directly related to the parameters of the three elements. If these relations are rearranged, it is possible to determine the mechanical parameters of the PDE from biological muscle experiments:

$$R_{\mathrm{PDE}} = \frac{A}{A + F_{\mathrm{AE,max}}}, \tag{11}$$

$$(1-\kappa_v) \cdot D_{\mathrm{PDE,max}} = \frac{A + F_{\mathrm{AE,max}}}{B}. \tag{12}$$

Here, the possible internal movement at the connection point of the elements introduces an additional degree of freedom, which has not been considered in Hill-type muscle models so far, except Ref. [53]. This degree of freedom is represented by κ_v, the gearing ratio (Eq. (3)). Isotonic quick release experiments, which are usually performed with biological muscles, are designed to eliminate the contribution of the serial elasticity. Therefore, it can be assumed that the SE is at constant length ($\dot{l}_{\mathrm{SE}} = 0$) in the experiment and hence, $\kappa_v = 0$.

With this assumption, the damper parameters can be determined. For this study, experimental data of a rat gastrocnemius muscle were used: $F_{\mathrm{AE,max}} = 13.39$ N and the Hill constants are $A = 2.68$ N and $B = 4.16 \times 10^{-2}$ m·s^{-1}

(Animal 1 in Ref. [12]). The resulting parameters are

$$R_{\mathrm{PDE}} = 0.17,$$

$$D_{\mathrm{PDE,max}} = 386.4\ \mathrm{N \cdot s \cdot m^{-1}}.$$

2.3 Numerical model

The numerical model of the CE can be expressed by two coupled differential equations. The first describes the internal movement (coordinate y_1 representing l_{AE}) based on Eqs. (1) and (4):

$$\dot{y}_1 = \frac{F_{\mathrm{SE}} - F_{\mathrm{AE}}}{d_{\mathrm{PDE}}(F_{\mathrm{CE}})}. \tag{13}$$

For the external movement (coordinate y_2 representing l_{CE}) two possible scenarios are considered:

(a) An isotonic contraction against a constant external force F_{ext} = const. Here, F_{ext} determines the length of the SE via $F_{\mathrm{ext}} = F_{\mathrm{SE}} = -k_{\mathrm{SE}}(l_{\mathrm{SE}} - l_{\mathrm{SE},0})$. Hence, l_{SE} = const and therefore

$$\dot{y}_2 = \dot{y}_1, \tag{14}$$

(b) A contraction against an inertial mass m at the end of the CE (y_2) is described by the differential equation

$$\ddot{y}_2 = g + \frac{1}{m} F_{\mathrm{SE}}, \tag{15}$$

where $g = 9.81\ \mathrm{m \cdot s^{-2}}$ is the gravitational acceleration.

For the SE a linear spring was chosen with

$$F_{\mathrm{SE}} = \begin{pmatrix} -k_{\mathrm{SE}} \cdot \Delta l_{\mathrm{SE}} & \Delta l_{\mathrm{SE}} > 0 \\ 0 & \Delta l_{\mathrm{SE}} \le 0 \end{pmatrix}, \tag{16}$$

where $k_{\mathrm{SE}} = 2401\ \mathrm{N \cdot m^{-1}}$ is the spring constant (in accordance to the mechanical setup), $\Delta l_{\mathrm{SE}} = y_2 - y_1 - l_{\mathrm{SE},0}$, and $l_{\mathrm{SE},0}$ the slack length of the spring.

This set of differential equations was solved with Matlab Simulink embedded ODE45 (Dormand-Prince) solver with absolute and relative tolerance of 1×10^{-7}.

2.4 Hardware model

AE and PDE: The force characteristics of the PDE and AE (Eqs. (4) and (6)) were implemented with an electric motor (Maxon ECmax40) as hardware in the loop in a Matlab Simulink environment through Real Time Workshop and Real Time Windows Target at 1 kHz sampling frequency (Fig. 2). The motor torque was controlled by Maxon digital EC-motor control units (DEC 70/10).

A disc with radius $r_{\mathrm{disk}} = 6$ mm was used to coil up a steel rope connected to the SE and thus exerted a force $F_{\mathrm{AE}} + F_{\mathrm{PDE}} = r_{\mathrm{disk}} \cdot T_{\mathrm{Motor}}$ on the SE. The force characteristics of the PDE and AE (Eqs. (4) and (6)) were implemented in Matlab Simulink through Real Time Workshop and Real Time Windows Target. In this way the motor could exert the specified force on the steel rope and the SE, as required by the theoretical construct. This was validated for the range of torques and speeds occurring during the experiments (current controller bandwidth ≈ 1 kHz, motor included >100 Hz, peak target frequencies ≈ 30 Hz).

SE: a linear metal spring ($k_{\mathrm{SE}} = 2401\ \mathrm{N \cdot m^{-1}}$) was tied to the steel rope.

Sensors: the motor shaft angular position φ_{Motor} was recorded by an optical encoder (Scancon 2RMHF 5000 pulses/revolution) and represented $y_1 = 2 r_{\mathrm{disk}} \varphi_{\mathrm{Motor}}$. An optical linear position encoder (Renishaw RGH24D 5 μm resolution) recorded y_2. A load cell (Transducer Techniques MLP 25 with amplifier TM0-1-24) recorded the force F_{CE}. All sensor data were recorded with Matlab Simulink via a Sensoray 626 AD I/O at 1 kHz.

Test-bed: Two experimental conditions were realized: (a) For isotonic contractions another motor was attached to the end of the spring to exert a constant external force $F_{\mathrm{ext}} = F_{\mathrm{CE}}$. (b) A variable weight was attached to the SE via a wheel at the end of the table. An electromagnet was installed to restrain the movement of the artificial CE end for isometric and quick release experiments.

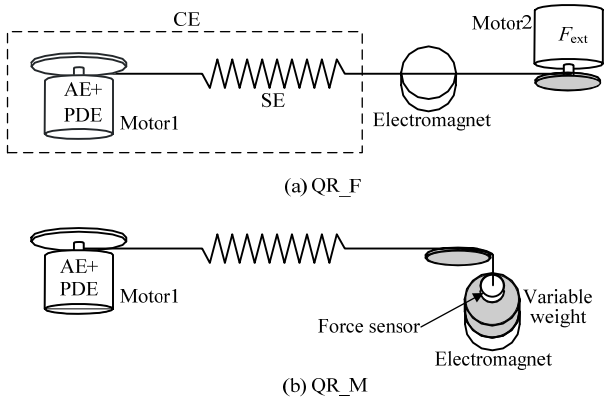

Fig. 2 Hardware design. AE and PDE forces were generated by an electric motor as hardware in the loop. SE was implemented as a mechanical spring. An electromagnet was used to fix the CE length in the isometric part of the quick release contractions. (a) For the QR_F experiments (isotonic), a second motor was used to generate a defined external force F_{ext}; (b) for the QR_M experiments (against an inertial mass M) a variable weight was used as load. The force sensor measured the CE force F_{CE}.

2.5 Experimental protocol

To investigate the force-velocity characteristics of the CE two experiments were performed. For both experiments, the AE activity was set to $q_{AE} = 1$ (maximum activity) and the CE length was fixed with the electromagnet in the beginning. This resulted in an AE/PDE contraction and a SE expansion until $F_{CE} = F_{AE,max}$. After this initial isometric contraction at $t_{QR} = 3$ s, the electromagnet was released. Then the whole CE started to contract and the two external conditions resulted in the two different experiments: Isotonic quick release contraction experiments (QR_F): Here, the CE contracted against a constant external force F_{ext}. External forces between 0.2 N$<F_{CE}<F_{AE,max}$ were applied in 19 steps. Each force condition was repeated ten times. The contraction velocity was evaluated 0.5 s after the release. For the quick release contraction against an inertial mass M (QR_M) the weight was released and CE contraction velocity and force were recorded[54]. Here, the force-velocity relation was extracted from the recorded data at the peak contraction velocity v_{max}.

3 Results

3.1 Isotonic quick release experiments

Isotonic quick-release experiments against a constant force (QR_F) revealed a hyperbolic force-velocity relation for the numerical model and the hardware implementation (Fig. 3). The numerical force-velocity relation was identical to the analytical prediction and to the fit of the biological muscle data[12] from which the model parameters were derived. This force-velocity relation is also shown in all other figures for reference (theory/biology, red line). The force-velocity data of the hardware implementation (green ×) shows a slight deviation towards lower velocities and lower forces. Fitting Eq. (7) to the data (with $\kappa_v = 0$) results in parameter estimates of $D_{PDE,max,fit} = 474$ N·s·m^{-1} and $R_{PDE,fit} = 0.15$ (goodness of fit: $R^2 = 0.96$), compared to the nominal values $D_{PDE,max} = 386$ N·s·m^{-1} and $R_{PDE} = 0.17$ preset from theory (Section **2.2**).

3.2 Quick release experiments against an inertial mass

Quick-release contractions against an inertial mass (QR_M) resulted in a different force-velocity relation with substantially higher contraction velocities (Fig. 4) compared to the isotonic quick-release contractions (Fig. 3). A hyperbolic fit ($R^2 = 0.80$) to the experimental data (green line) gives parameter estimates of $D_{PDE,max,fit} = 162$ N·s·m^{-1} and $R_{PDE,fit} = 0.14$, although the nominal damper parameters were kept identical to those of the QR_F experiments.

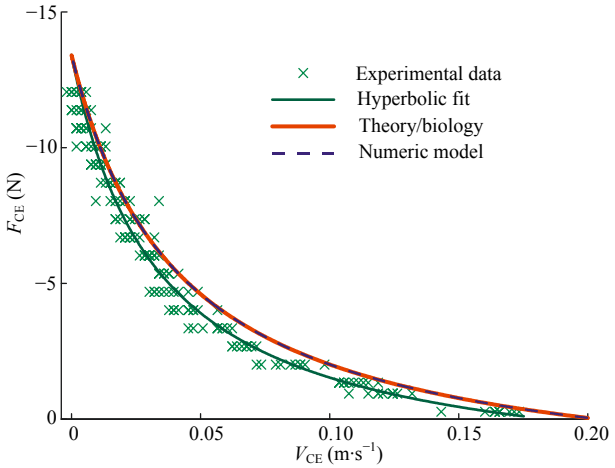

Fig. 3 Force-velocity relation determined in isotonic quick release experiments (QR_F). The numerical simulation (blue dashed line) resulted in a force-velocity relation identical to the theoretical prediction of the analytical model (red solid line). A fit (green solid line, $R^2 = 0.96$) to the experimental data (green ×) revealed a hyperbolic force-velocity relation also for the hardware model. The deviation between the theoretical prediction of the analytical model and the fit of the experimental data was probably the result of additional internal friction (motors, bearings), which caused a reduction in the contraction velocities and AE forces.

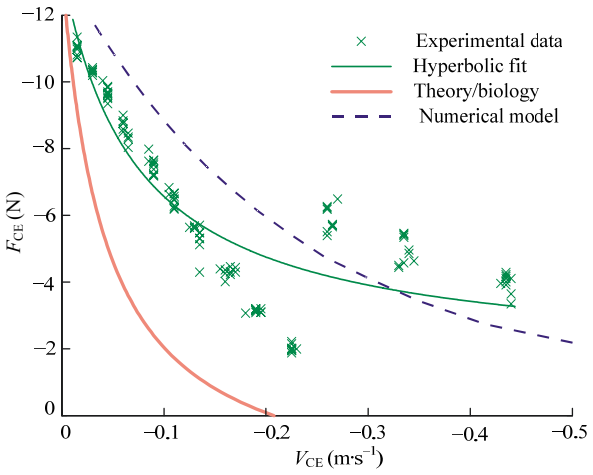

Fig. 4 Quick release experiments against an inertial mass (QR_M). The force-velocity relation was determined by finding the time index with highest contraction velocity v_{max} and by extracting velocity and force at this time index for each experiment. These data points plotted (and connected, or fitted) represent the force-velocity relation $F_{CE}(v_{max})$. The numerical simulation (blue dashed line) resulted in a force-velocity relation with substantially higher velocities than the QR_F simulations. The experimental data (green ×) and a hyperbolic fit (green solid line, $R^2 = 0.80$) for the hardware model showed a similar trend to higher velocities. The theoretical prediction of the analytical model for $\kappa_v = 0$ isotonic experiments (red line) is drawn for reference.

The experimental force vs. velocity trajectories show additional oscillations (Fig. 5), which are not present in the simulation (Fig. 6). These oscillations originate from additional masses and elasticities introduced by force/position sensor and steel wire connections respectively. The peculiar step in the experimental force-velocity relation (Fig. 4) is a result of these additional oscillations. As shown in Fig. 5, there are two prominent maxima in the velocity. For increasing masses, at one point the second maximum becomes the absolute maximum which corresponds to a lower force and therefore results in the step in the force-velocity relation.

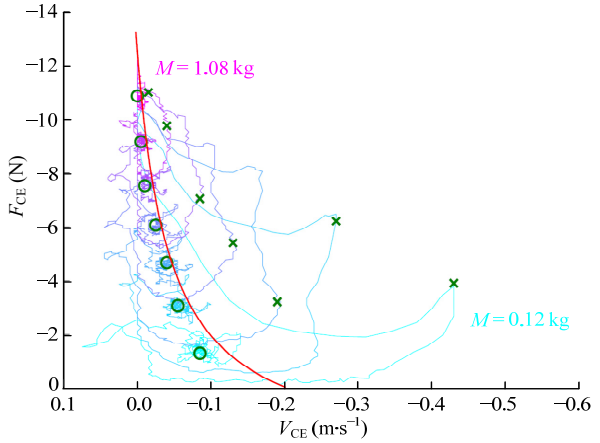

Fig. 5 Experimental time course of the force-velocity relation in QR_M experiments against varying inertial masses. The color of the line indicates the mass (small mass: light blue, heavy mass: pink). Every experiment starts at $v_{CE} = \dot{l}_{CE} = 0$ and $F_{CE} = F_{AE,max} =$ 13.39 N. The absolute maximum in the velocity v_{max} is detected for the force-velocity relation and marked with ×. These maxima describe the force-velocity relation determined in QR_M experiments. The long time convergence points of the force-velocity trajectories are marked with black O. These convergence points lie close on the force-velocity relation determined by QR_F experiments.

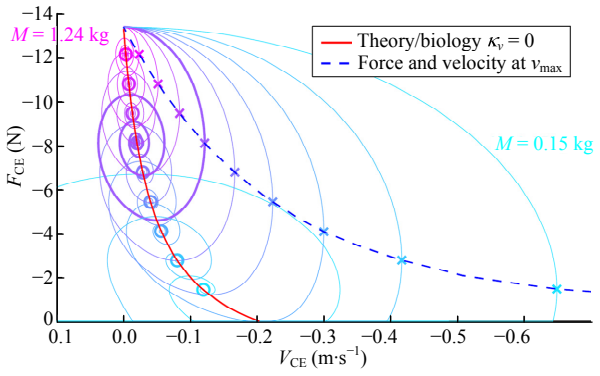

Fig. 6 Simulated time course of the force-velocity relation in QR_M experiments. The color of the line indicates the mass (small mass: light blue, heavy mass: pink). Every experiment starts at $v_{CE} = \dot{l}_{CE} = 0$ and $F_{CE} = F_{AE,max} =$ 13.39 N (upper left corner). From there, the contraction velocity increases up to a maximum v_{max} marked with ×. Connecting these maxima gives the force-velocity relation determined in QR_M experiments (blue dashed line). The long time convergence points of the force-velocity trajectories are marked with O. These convergence points lie on the force-velocity relation determined by QR_F simulations (red line).

4 Discussion and conclusion

In a bionic approach, the function and structure of muscle in quick release experiments were investigated. A new macroscopic model was presented that analytically predicts the hyperbolic force-velocity relation known to characterize the contraction dynamics of active fibers and their assemblies in biological muscles. It was the goal of this study to understand the relationship between the macroscopic model structure and its dynamic role in the contraction. To that end, two types of quick release contraction experiments were performed with a numerical model and a hardware implementation. Both, the numerical model and the hardware implementation confirmed the analytical model.

These results prove that the origin of the hyperbolic force-velocity relation can be mechanically explained on a macroscopic level by the arrangement of the three mechanical elements AE, PDE and SE[53]. If the CE is considered to be the active engine of the muscle, the analytical model predicts its operating points and the numerical model presents differential equations to predict the dynamic force generation of the CE. In contrast to microscopic muscle models, where the hyperbolic force-velocity relation is explained in terms of cross-bridge state and related transition rates and chemical rates[15–23], it is here explained in terms of fundamental macroscopic mechanical properties. Still, it remains open where in detail the microscopic origin of the mechanical properties are located. Nevertheless, in distinction to other macroscopic Hill-type muscle models, the force-velocity relation is not implemented as an empirical function $F(v)$[1,2,14,26] but rather is the dynamical result of the interaction of mechanical elements. Therefore, this model can be seen as a macroscopic muscle model derived from first-order mechanical principles.

From our point of view, the advantages of the model are: (a) It is possible to investigate the contribution of the mechanical muscle characteristics, represented by AE, PDE, and SE, to the overall contraction

dynamics; (b) The force-velocity operating points can be predicted analytically for different contraction modes; (c) Biological experiments can be interpreted within the framework of the model; (d) As the model is based on mechanical elements, it could serve as a template for the construction of bionic artificial muscles with biological contraction dynamics.

4.1 Predictions between the extreme experimental conditions

In biological muscle experiments very specific contraction conditions are generated. Isotonic quick release experiments are designed to eliminate the contribution of the serial elasticities to the overall muscle contraction ($\dot{l}_{SE} = 0$) and thus, allowing to determine the force-velocity characteristics of the CE[2,10–12]. These conditions are consistent with a gearing ratio of $\kappa_v = 0$ (Eq. (3)). The force-velocity data determined under these conditions are then fitted with the hyperbolic Hill-equation (Eq. (8)) to determine the parameters A and B[1]. In order to derive the values of the parameters R_{PDE} and $D_{PDE,max}$ for our model from such a parameter set, an assumption about κ_v has to be made (see Eqs. (11) and (12)). Here $\kappa_v = 0$ was the logical choice as it corresponds to the original biological experiment. These parameters were then used in the numerical model and the hardware experiment. Performing isotonic quick release simulations and experiments and thus, reproducing the $\kappa_v = 0$ condition, resulted in the exact reproduction of the theoretical force-velocity relation (Fig. 3).

Quick release experiments against an inertial mass[13,14] on the other hand generated contractions with $\kappa_v \neq 0$. As expected, the force-velocity operating points in this case did not lie on the original force-velocity relation (Fig. 4). At the peak CE contraction velocity, where the force-velocity data were extracted[14], the contraction was mainly governed by the SE ($\kappa_v > 0.81$). This means that AE and PDE almost stay at constant length for the first part of the QR_M contraction. We compared this to a model with locked AE/PDE length, where only the SE spring accelerated the mass (see also appendix). This extreme case of $\kappa_v = 1$ results in a force-velocity relation very similar to the force-velocity relation of the QR_M experiments (gray line, Fig. 7).

During the QR_M contractions κ_v changed continuously. In fact, points could be extracted from the QR_M experiments, where κ_v reached certain specific values. Interestingly, all force-velocity operating points corresponding to a specific κ_v lie on a new hyperbola (Fig. 7). This hyperbola can be exactly predicted from the theory (Eqs. (8)–(10)). The surprising fact is that once the material properties $D_{PDE,max}$ and R_{PDE} are defined, the additional free parameter κ_v predicts every force-velocity operating point of the CE, independent of the experiment.

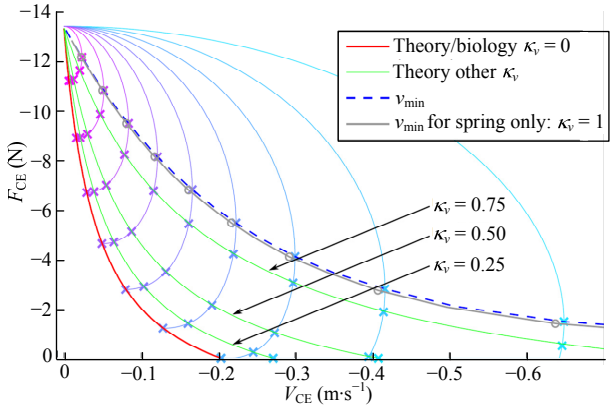

Fig. 7 During the time course of the contraction in QR_M experiments, the internal gearing ratio κ_v changes continuously. From the simulation data, points were extracted where κ_v reached a certain value (marked with ×). The theoretical prediction of the hyperbolic force-velocity relation on the other hand depends on the parameter κ_v. Plotting the theoretical predictions for the chosen κ_v values (green lines for $\kappa_v = 0.25$, $\kappa_v = 0.5$ and $\kappa_v = 0.75$) shows, that these operating points all correspond to one specific hyperbolic force-velocity relation (intersections of green lines with time traces of the experiment, marked with ×). The extreme case where all contraction happens in the SE ($\kappa_v = 1$) cannot be described by Eq. (8), as $B \to \infty$ for $\kappa_v \to 1$. But this condition can be described by the isolated contraction dynamics of the spring mass system (SE with external mass). The derivation is explained in the appendix and the results are plotted here (gray line).

Therefore, the two quick release experiments QR_F and QR_M can be seen as two extreme cases. In the QR_F experiments the SE does not contribute to the contraction, while in the QR_M it mainly determines the contraction. For normal biological movements, κ_v will lie in between ($0 < \kappa_v < 1$). The theory, the numeric model and the hardware implementation presented here, predict and reproduce the force-velocity operating points for all these situations.

The isotonic experiments show, that the specific damper characteristic chosen would provide already a hyperbolic force-velocity relationship without any serial

element as it does not contribute to the contraction (κ_v = 0). Therefore, our model implies on a mathematical level to "switch off the SE". Yet going beyond, our model also demonstrates that this property is inherited by any CE structure in which a further arbitrary force bearing element is plugged in serially, which adds an internal degree of freedom to the CE structure. By mechanical design, the CE structure, thus, gains a manifold of similar force-velocity relations. This also adds function to the structure, namely the potential to profit from the benefits of the force-velocity relation[2,10–12] during changing loading situations in the real world. Also, mechanical efficiency can be optimized across the whole range of loading situations[53]. For this, serial elasticity seems to be particularly beneficial. Our hardware prototype has demonstrated the real world functionality of such a specific implementation of the theoretical structure.

4.2 Interpreting biological experiments: muscle structure and κ_v

Both, in our technical prototype and our theoretical model, the internal degree of freedom represented by the parameter κ_v can distinguish between different loading modes, e.g., the extremes of an isotonic contraction or a quick-release contraction against an inertial load. Moreover, both approaches can deal with any in-between contraction as a cyclic work-loop, a stretch-shortening cycle, and an isovelocity or even an isometric contraction during a rise in activity. But does our theoretical model or our technical prototype really map physiological processes in the biological muscle during all these contraction modes?

On the one hand, from a theoretical point of view, we would expect at least slight differences in the results of isotonic and isovelocity experiments, even in a biological muscle. This is because the contraction velocity should immediately change, per definition, during an isotonic contraction. Consequently, the muscle examined is supposed to go through some finite length changes, even though they may be small. Therefore and also keeping muscle's well-known history effects in mind[55,56] when comparing both experimental conditions, the muscle is also supposed to go through a manifold of different states around the operating points examined. This should be reflected by slight differences in force-velocity or velocity-force, respectively, and force- or velocity-enthalpy relations, respectively.

On the other hand, when comparing our theoretical model calculations to enthalpy data of biological muscle, the model predicts a specific parameter value κ_v = 0.85 for the internal distribution of contraction velocities[57]. This very value is, however, not what would be expected in a real muscle assuming that the model SE represents just serial elastic properties of active muscle fibers. Since pure elastic structures would not change their length during a finite isotonic contraction, meaning κ_v = 0 (stationary SE length). Although the biological muscle data used for validation had been determined in the isovelocity rather than in the isotonic condition we would yet not expect such a discrepancy when comparing measurements from both conditions in the same muscle. Thus, answering the first part of the above question, our model needs further development.

Any elastic structure is slightly damped in reality. This is e.g. a necessity to suppress load-muscle eigen oscillations[14]. If, as a consequence of this damping, the SE was rather visco-elastic than purely elastic, better predictions of enthalpy production would be expected. Additionally, such a serial arrangement of dampers would automatically lead to history effects within the CE (active muscle). Furthermore, we would like to annotate that this would also mean that an often used assumption should be reconsidered: if there is some damping in any serial element then the isotonic condition does not guarantee that the SE is at constant length during isotonic quick-release experiments, i.e. κ_v>0. As a consequence, the measured force-velocity properties can not directly be related to the hypothesized AE in series. Rather, the isotonic measurements would reflect the entangled properties of the whole arrangement including the visco-elasticity of the SE itself, both when asking for the force-velocity characteristics and the heat production. In terms of our model, one would measure a hyperbolic force-velocity relation rather corresponding to one of the green curves in Fig. 7 than the desired red curve.

Answering the second part of the above question, our current technical prototype was designed to incorporate as low serial damping as possible, using an off-the-shelf spring as SE. However, neither have the damping characteristics of such a real spring been examined so far, although our measured data point to some additional damping in the prototype[54]. Nor is clear as of

today whether the built-in damping may suffice to represent potential serial damping of a real muscle. As presented, the latter should be predicted from an improved theoretical model to be validated with measured enthalpy data of biological muscles.

4.3 Model assumptions and extendability

This theory focuses on the mechanical origin of the force-velocity relation. Other important features of the muscle contraction dynamics, such as the force-length relation[3,4,58–61], force enhancement and contraction history effects[56,62–65], activation dynamics[24], *etc*. are neglected. However, we expect that including these characteristics in a similar way as it has been done previously in Hill-type models, would enhance the model without principally altering the force-velocity characteristics presented here. The AE force (Eq. (6)) for example may depend on AE or CE length. Here we basically only consider the state in which the CE operates at its optimal length. AE force could also depend on muscle activity and the chemical state of the muscle, i.e. the relative number of actively force-producing cross-bridges quantified by the normalized muscle activity $0 \leq q_{AE} \leq 1$.

The hardware experiment represented AE and PDE combined by a software controlled motor exerting a calculated force on the SE. With respect to a more adequate mechanical representation, we already separated AE and PDE in Ref. [54] by using one separate motor for each element. This made no difference for the QR_M experiments investigated there. In a next step, a real mechanical implementation of the PDE e.g. by a magneto-rheological damper[66], would be desirable. Also the AE could in principle be any other force generating device/material. Nevertheless, the hardware representation of AE and PDE in this paper is the simplest possible physical implementation. In the bionic context this step is necessary to verify the real world functionality of the concept[67].

4.4 Advantages of biological muscle system design

When looking at the complexity and variety of movements that biological muscles can generate, it is shown that biological muscle is a versatile, powerful, and flexible actuator[68]. Muscles are said to have benefits for the generation and the control of biological movements compared to known (classical) technical actuators[69]. They are thought to operate energy efficient, have intrinsic properties that have inherently stabilizing effects, and reduce the control effort[70]. This is achieved because muscles can operate in different modes depending on the loading situation and the structural implementation[71]. From a robotics and prosthetics point of view, it would be desirable to have an artificial actuator with similar capabilities[46,72]. However, in order to transfer these advantages to technical systems it is necessary to (a) determine the characteristics uniquely identifying the biological muscle and (b) evaluate the system design criteria with quantitative and comparable measures.

In the light of our findings we can contribute to (a): at least three basic mechanical characteristics of a biological muscle are necessary to exhibit muscle-like contraction dynamics: (i) a serial structure, with an active part in series to at least one visco-elastic part; (ii) a serial structure in which each part contains some low damping; (iii) a structural assembly including one force-dependent damping part, no matter in which branch of the serial structure. A first simple solution of a bio-inspired functional artificial muscle based on these characteristics was described in Ref. [57]. In this context, our model can be seen as a design template for functional artificial muscles.

In order to pinpoint the specific design criteria as demanded in (b) we propose several quantitative measures. In accordance with the postulated advantages of biological muscles the mechanical efficiency, heat production and enthalpy rates during natural movements are important criteria. Furthermore, stability and robustness of muscularly driven movements against internal and external perturbations and the related control effort should be quantified. We expect that only an integrative view of all these measures will allow to prove the accuracy of muscle models, pinpoint the design criteria for artificial muscles and quantitatively specify the advantages of biological and bio-inspired muscle system design.

Acknowledgments

This work was supported by a Research Seed Capital (RiSC) - Tranche 2009 from the Ministry of Science, Research and Arts of Baden-Württemberg and the University of Stuttgart (Kapitel 1403 Tit.Gr. 74).

References

[1] Hill A V. The heat of shortening and the dynamic constants of muscle. *Proceedings of the Royal Society of London*: *Series B*, 1938, **126**, 136–195.

[2] Ettema G J C, Huijing P A. Isokinetic and isotonic force-velocity characteristics of rat EDL at muscle optimum length. In Groot G D, Hollander A P, Huijing P A, Van Ingen Schenau G J (eds.) *Biomechanics XI-A*, Free University Press, Amsterdam, 1988, 58–62.

[3] Rassier D E, MacIntosh B R, Herzog W. Length dependence of active force production in skeletal muscle. *Journal of applied physiology*, 1999, **86**, 1445–1457.

[4] Bobbert M F, Ettema G C, Huijing P A. The force-length relationship of a muscle-tendon complex: Experimental results and model calculations. *European Journal of Applied Physiology and Occupational Physiology*, 1990, **61**, 323–329.

[5] Gordon A M, Huxley A F, Julian F J. The variation in isometric tension with sarcomere length in vertebrate muscle fibres. *The Journal of physiology*, 1966, **184**, 170–192.

[6] Bressler B H, Clinch N F. The compliance of contracting skeletal muscle. *The Journal of physiology,* 1974, **237**, 477–493.

[7] Barclay C J, Constable J K, Gibbs C L. Energetics of fast- and slow-twitch muscles of the mouse. *The Journal of physiology*, 1993, **472**, 61–80.

[8] Siebert T, Rode C, Herzog W, Till O, Blickhan R. Nonlinearities make a difference: Comparison of two common Hill-type models with real muscle. *Biological Cybernetics*, 2008, **98**, 133–143.

[9] Till O, Siebert T, Rode C, Blickhan R. Characterization of isovelocity extension of activated muscle: A Hill-type model for eccentric contractions and a method for parameter determination. *Journal of Theoretical Biology*, 2008, **255**, 176–187.

[10] Jewell B R, Wilkie D R. An analysis of the mechanical components in frog's striated muscle. *The Journal of Physiology*, 1958, **143**, 515–540.

[11] Cavagna G A, Citterio G. Effect of stretching on the elastic characteristics and the contractile component of frog striated muscle. *The Journal of Physiology*, 1974, **239**, 1–14.

[12] van Zandwijk J P, Bobbert M F, Baan G C, Huijing P A. From twitch to tetanus: Performance of excitation dynamics optimized for a twitch in predicting tetanic muscle forces. *Biological Cybernetics*, 1996, **75**, 409–417.

[13] Wilkie D R. The relation between force and velocity in human muscle. *The Journal of Physiology*, 1949, **110**, 249–280.

[14] Günther M, Schmitt S, Wank V. High-frequency oscillations as a consequence of neglected serial damping in Hill-type muscle models. *Biological Cybernetics*, 2007, **97**, 63–79.

[15] Huxley A F. Muscle structure and theories of contraction. *Progress in Biophysics and Biophysical Chemistry*, 1957, **7**, 255–318.

[16] Huxley A F. A note suggesting that the cross-bridge attachment during muscle contraction may take place in two stages. *Proceedings of the Royal Society of London*: *Series B*, 1973, **183**, 83–86.

[17] Cooke R, White H, Pate E. A model of the release of myosin heads from actin in rapidly contracting muscle fibers. *Biophysical Journal*, 1994, **66**, 778–788.

[18] Piazzesi G, Lombardi V. A cross-bridge model that is able to explain mechanical and energetic properties of shortening muscle. *Biophysical Journal*, 1995, **68**, 1966–1979.

[19] Piazzesi G, Lombardi V. Simulation of the rapid regeneration of the actinmyosin working stroke with a tight coupling model of muscle contraction. *Journal of Muscle Research and Cell Motility*, 1996, **17**, 45–53.

[20] Barclay C J. A weakly coupled version of the Huxley crossbridge model can simulate energetics of amphibian and mammalian skeletal muscle. *Journal of Muscle Research and Cell Motility*, 1999, **20**, 163–176.

[21] Chin L, Yue P, Feng J J, Seow C Y. Mathematical simulation of muscle cross-bridge cycle and force-velocity relationship. *Biophysical Journal*, 2006, **91**, 3653–3663.

[22] Lan G, Sun S X. Dynamics of myosin-driven skeletal muscle contraction: I. Steady-state force generation. *Biophysical Journal*, 2005, **88**, 4107–4117.

[23] Walcott S, Sun S X. Hysteresis in cross-bridge models of muscle. *Physical Chemistry Chemical Physics*: *PCCP*, 2009, **11**, 4871–4881.

[24] Zajac F E. Muscle and tendon: Properties, models, scaling, and application to biomechanics and motor control. *Critical Reviews in Biomedical Engineering*, 1989, **17**, 359–411.

[25] Winters J M. Hill-based muscle models: A systems engineering perspective. In Winters J M, Woo S Y (eds), *Multiple Muscle Systems*: *Biomechanics and Movement Organization*, Springer-Verlag Berlin and Heidelberg, New York, 1990, 69–93.

[26] van Soest A J, Bobbert M F. The contribution of muscle properties in the control of explosive movements. *Biological Cybernetics*, 1993, **69**, 195–204.

[27] Hatze H. The complete optimization of a human motion. *Mathematical Biosciences*, 1976, **28**, 99–135.

[28] Pandy M G, Zajac F E, Sim E, Levine W S. An optimal

control model for maximum-height human jumping. *Journal of Biomechanics*, 1990, **23**, 1185–1198.

[29] Günther M, Ruder H. Synthesis of two-dimensional human walking: A test of the lambda-model. *Biological Cybernetics*, 2003, **89**, 89–106.

[30] Geyer H, Herr H. A muscle-reflex model that encodes principles of legged mechanics produces human walking dynamics and muscle activities. *IEEE Transactions on Neural Systems and Rehabilitation*, 2010, **18**, 263–273.

[31] Bobbert M F, Casius L J R. Spring-like leg behaviour, musculoskeletal mechanics and control in maximum and submaximum height human hopping. *Philosophical Transactions of the Royal Society of London*: *Series B*, 2011, **366**, 1516–1529.

[32] Happee R. Inverse dynamic optimization including muscular dynamics, a new simulation method applied to goal directed movements. *Journal of Biomechanics*, 1994, **27**, 953–960.

[33] Erdemir A, McLean S, Herzog W, van den Bogert A J. Model-based estimation of muscle forces exerted during movements. *Clinical Biomechanics*, 2007, **22**, 131–154.

[34] Gerritsen K G M, van Den Bogert A J, Hulliger M, Zernicke R F. Intrinsic muscle properties facilitate locomotor control – a computer simulation study. *Motor Control*, 1998, **2**, 206–220.

[35] Geyer H, Seyfarth A, Blickhan R. Positive force feedback in bouncing gaits? *Proceedings of the Royal Society of London*: *Series B*, 2003, **270**, 2173–2183.

[36] van der Krogt M M, de Graaf W W, Farley C T, Moritz C T, Casius L J R, Bobbert M F. Robust passive dynamics of the musculoskeletal system compensate for unexpected surface changes during human hopping. *Journal of Applied Physiology*, 2009, **107**, 801–808.

[37] Haeufle D F B, Grimmer S, Seyfarth A. The role of intrinsic muscle properties for stable hopping–stability is achieved by the force–velocity relation. *Bioinspiration & Biomimetics*, 2010, **5**, 016004 (11pp).

[38] Ettema G C. Effects of contraction history on control and stability in explosive actions. *Journal of Electromyography and Kinesiology*, 2002, **12**, 455–461.

[39] Alexander R M. Three uses for sSprings in legged locomotion. *The International Journal of Robotics Research*, 1990, **9**, 53–61.

[40] Lindstedt S L, LaStayo P C, Reich T E. When active muscles lengthen: Properties and consequences of eccentric contractions. *News in Physiological Sciences*, 2001, **16**, 256–261.

[41] Blickhan R, Seyfarth A, Geyer H, Grimmer S, Wagner H, Günther M. Intelligence by mechanics. *Philosophical Transactions of the Royal Society of London*: *Series A*, 2007, **365**, 199–220.

[42] Schmitt S, Günther M. Human leg impact: Energy dissipation of wobbling masses. *Archive of Applied Mechanics*, 2010, **81**, 887–897.

[43] Raibert M H. Legged robots. *Communications of the ACM*, 1986, **29**, 499–514.

[44] Webb B. Using robots to model animals: A cricket test. *Robotics and Autonomous Systems*, 1995, **16**, 117–134.

[45] Atkeson C G, Hale J G, Pollick F, Riley M, Kotosaka S, Schaul S, Shibata T, Tevatia G, Ude A, Vijayakumar S, Kawato E, Kawato M. Using humanoid robots to study human behavior. *IEEE Intelligent Systems and Their Applications*, 2000, **15**, 46–56.

[46] Dillmann R, Albiez J, Gassmann B, Kerscher T, Zöllner M. Biologically inspired walking machines: design, control and perception. *Philosophical Transactions of the Royal Society of London*, *Series A*, 2007, **365**, 133–151.

[47] Pfeifer R, Lungarella M, Iida F. Self-organization, embodiment, and biologically inspired robotics. *Science*, 2007, **318**, 1088–1093.

[48] Ijspeert A J, Crespi A, Ryczko D, Cabelguen J-M. From swimming to walking with a salamander robot driven by a spinal cord model. *Science*, 2007, **315**, 1416–1420.

[49] Pratt G A, Williamson M M. Series elastic actuators. *Proceedings* 1995 *IEEE/RSJ International Conference on Intelligent Robots and Systems*, Pittsburgh, Pennsylvania, USA, 1995, 399–406.

[50] Hannaford B, Jaax K, Klute G K. Bio-inspired actuation and sensing. *Autonomous Robots*, 2001, **11**, 267–272.

[51] Albu-Schäffer A, Eiberger O, Grebenstein M, Haddadin S, Ott C, Wimböck T, Wolf S, Hirzinger G. Soft robotics. *IEEE Robotics & Automation Magazine*, 2008, **15**, 20–30.

[52] Hurst J, Rizzi A. Series compliance for an effcient running gait. *IEEE Robotics & Automation Magazine*, 2008, **15**, 42–51.

[53] Günther M, Schmitt S. A macroscopic ansatz to deduce the Hill relation. *Journal of Theoretical Biology*, 2010, **263**, 407–418.

[54] Haeufle D F B, Günther M, Blickhan R, Schmitt S. Proof of concept: Model based bionic muscle with hyperbolic force-velocity relation. *Applied Bionics and Biomechanics*, 2012, published online.

[55] Abbott B C, Aubert X M. The force exerted by active striated muscle during and after change of length. *The Journal of Physiology*, 1952, **117**, 77–86.

[56] Rode C, Siebert T, Blickhan R. Titin-induced force enhancement and force depression: A "sticky-spring" mecha-

nism in muscle contractions? *Journal of Theoretical Biology*, 2009, **259**, 350–360.

[57] Schmitt S, Haeufle D F B, Blickhan R, Günther M. Nature as an engineer: One simple solution of a bio-inspired functional artificial muscle. *Bioinspiration & Biomimetics*, 2012, in review.

[58] van Ingen Schenau G J, Bobbert M F, Ettema G C, de Graaf J B, Huijing P A. A simulation of rat edl force output based on intrinsic muscle properties. *Journal of Biomechanics*, 1988, **21**, 815–824.

[59] Durfee W K, Palmer K I. Estimation of force-activation, force-length, and force-velocity properties in isolated, electrically stimulated muscle. *IEEE Transactions on Bio-Medical Engineering*, 1994, **41**, 205–216.

[60] Zuurbier C J, Heslinga J W, Lee-de Groot M B E, van der Laarse W J. Mean sarcomere length-force relationship of rat muscle fibre bundles. *Journal of Biomechanics*, 1995, **28**, 83–87.

[61] Rode C, Siebert T, Herzog W, Blickhan R. The effects of parallel and series elastic components on the active cat soleus force-length relationship. *Journal of Mechanics in Medicine and Biology*, 2009, **9**, 105–122.

[62] Forcinito M, Epstein M, Herzog W. Can a rheological muscle model predict force depression/enhancement? *Journal of Biomechanics*, 1998, **31**, 1093–1099.

[63] Meijer K, Grootenboer H J, Koopman H F J M, van der Linden B J J J, Huijing P A. A Hill type model of rat medial gastrocnemius muscle that accounts for shortening history effects. *Journal of Biomechanics*, 1998, **31**, 555–563.

[64] Herzog W, Leonard T R. Force enhancement following stretching of skeletal muscle: A new mechanism. *The Journal of Experimental Biology*, 2002, **205**, 1275–1283.

[65] Herzog W. History dependence of skeletal muscle force production: Implications for movement control. *Human Movement Science*, 2004, **23**, 591–604.

[66] Garcia E, Arevalo J, Muñoz G, Gonzalez-de Santos P. Combining series elastic actuation and magneto-rheological damping for the control of agile locomotion. *Robotics and Autonomous Systems*, 2001, **59**, 827–839.

[67] Nachtigall W. *Bionik*, 2nd ed, Springer, Berlin, Germany, 2002.

[68] McMahon T A. *Muscles*, *Reflexes*, *and Locomotion*, Princeton University Press, Princeton, NJ, USA, 1984.

[69] Ritzmann R E, Quinn R D, Watson J T, Zill S N. Insect walking and biorobotics: A relationship with mutual benefits. *BioScience*, 2000, **50**, 23–33.

[70] Grimmer S, Ernst M, Günther M, Blickhan R. Running on uneven ground: Leg adjustment to vertical steps and self-stability. *The Journal of Experimental Biology*, 2008, **211**, 2989–3000.

[71] Lieber R L. Skeletal muscle is a biological example of a linear electroactive actuator. *Proceedings of SPIE's 6th Annual International Symposium on Smart Structures and Materials*, 1999, **3669**, 19–25.

[72] Baughman R H. Playing nature's game with artificial muscles. *Science*, 2005, **308**, 63–65.

Appendix

Force- and load-velocity relations of a spring-mass system during quick-release

Here, we demonstrate that a system of a pre-loaded linear spring which accelerates an inertial mass M during a quick-release situation exhibits a non-linear, hyperbolic-like load-velocity relation. The "load" may be either just the mass M or the weight $M{\cdot}G$ in case the mass is also exposed to gravity, with G denoting the absolute value of the gravitational acceleration.

Let t symbolize the time, d/dt a time derivation, x the coordinate along which the spring is stretched and the mass is displaced, K the spring stiffness, and x_s the rest length of the spring at which its force

$$F_s = -K(x - x_s) = -K\Delta x, \tag{A1}$$

is zero. There are three contributions to the energy E of the system:

$$E_s(t) = \frac{1}{2} K \Delta x^2(t), \tag{A2}$$

$$E_G(t) = -MG\Delta x(t), \tag{A3}$$

$$E_v(t) = \frac{1}{2} M v^2(t), \tag{A4}$$

where E_s denotes the potential energy stored in the spring, E_G the potential energy of the mass due to gravity, and E_v its kinetic energy when moving with velocity $v = \frac{\mathrm{d}x(t)}{\mathrm{d}t} = \frac{\mathrm{d}\Delta x(t)}{\mathrm{d}t}$. The energy of the system characterized by the equation of motion

$$M \frac{\mathrm{d}^2 x(t)}{\mathrm{d}t^2} = M \frac{\mathrm{d}^2 \Delta x(t)}{\mathrm{d}t^2} = F_s(t) + MG = -K\Delta x(t) + MG, \tag{A5}$$

is conserved:

$$E = E_s + E_G + E_v = E_0 = \frac{1}{2} K \Delta x_0^2 - MG\Delta x_0 + \frac{1}{2} M v_0^2. \tag{A6}$$

We identify the initial value of a variable (at $t = 0$) by the index "0". For reasons of conciseness and further on, we omit the symbol "(t)" for the time-dependency of the variables Δx and thus, F_s, E_s, E_G, E_v. Now, when substituting the spring force F_s from Eq. (A1) into the terms E_s and E_G on left hand side of Eq. (A6) we find that the latter constitutes the instantaneous non-linear (spring) force-velocity relation

$$F_s^2 + 2MGF_s + KMv^2 - 2KE_0 = 0, \tag{A7}$$

which can be solved for, e.g., the force

$$F_s = -MG \pm \sqrt{(MG)^2 + 2KE_0 - Kv^2}. \tag{A8}$$

The mass reaches its maximum velocity $v_{\max}$ during spring contraction when the spring force F_s just compensates weight force MG. In this condition, the square root term must vanish, that is, we find

$$v_{\max}(M, x_{0,0}) = -\frac{1}{\sqrt{KM}} \sqrt{(MG)^2 + 2KE_0}. \tag{A9}$$

In analogy to the force-velocity relation of a CE, which represents the velocity response of a CE to a given external force (or vice versa), Eq. (A9) is the load-velocity relation characterizing the velocity response of the spring-mass system when the load (M or MG) is varied. Due to the square root in the denominator the course of this load-velocity relation resembles a hyperbola which has an intersection with the load axis ($v_{\max} = 0$). However, in contrast to a CE force-velocity relation, $v_{\max}$ becomes infinite for a vanishing load, i.e., the load-velocity relation just aligns asymptotically with the velocity axis, a corresponding global $v_{\max,M=0}$ does not occur.

Usually, the mass is at rest in the instant of release ($v_0 = 0$). In that case, the energy content $E = E_0$ of the system (Eq. (A6)) can be written as

$$E_0 = \frac{1}{2} K \Delta x_0^2 - MG\Delta x_0 = \frac{1}{K}\left(\frac{1}{2} F_{s,0}^2 - MGF_{s,0}\right), \tag{A10}$$

where we have substituted the initial force $F_{s,0} = -K\Delta x_0$ (maximum force during spring contraction) to get the latter notation. Then, the maximum velocity reached during contraction (Eq. (A9)) is simply

$$v_{\max}(M, x_0) = -\frac{F_{s,0} - MG}{\sqrt{KM}}. \tag{A11}$$